ORIGINAL PAPER

Spherical indentation method for determining the constitutive parameters of hyperelastic soft materials

Man-Gong Zhang · Yan-Ping Cao · Guo-Yang Li · Xi-Qiao Feng

Abstract A comprehensive study on the spherical indentation of hyperelastic soft materials is carried out through combined theoretical, computational, and experimental efforts. Four widely used hyperelastic constitutive models are studied, including neo-Hookean, Mooney–Rivlin, Fung, and Arruda–Boyce models. Through dimensional analysis and finite element simulations, we establish the explicit relations between the indentation loads at given indentation depths and the constitutive parameters of materials. Based on the obtained results, the applicability of Hertzian solution to the measurement of the initial shear modulus of hyperelastic materials is examined. Furthermore, from the viewpoint of inverse problems, the possibility to measure some other properties of a hyperelastic material using spherical indentation tests, e.g., locking stretch, is addressed by considering the existence, uniqueness, and stability of the solution. Experiments have been performed on polydimethylsiloxane to validate the conclusions drawn from our theoretical analysis. The results reported in this study should help identify the extent to which the mechanical properties of hyperelastic materials could be measured from spherical indentation tests.

Keywords Spherical indentation · Hyperelastic soft materials · Dimensional analysis · Finite element method · Inverse problem

1 Introduction

Understanding the deformation behavior of soft materials such as elastomeric materials and biological soft tissues has

M.-G. Zhang · Y.-P. Cao (✉)· G.-Y. Li · X.-Q. Feng
AML, Department of Engineering Mechanics, Tsinghua University, Beijing 100084, China
e-mail: caoyanping@tsinghua.edu.cn

received considerable attention during past years. Due to their intrinsic features of low elastic moduli and high sensitivity to external stimuli, soft materials often undergo large deformation and exhibit strong nonlinear responses. Determining the mechanical properties of these materials is of great importance, for instance, for tissue engineering as well as for understanding growth-induced large deformation behavior of soft tissues (Rodriguez et al. 1994; Taber 1995; Ben Amar and Goriely 2005; Li et al. 2012) and the responses of cells or tissues to various external stimuli (Humphrey 2003; Holzapfel and Ogden 2006; Levental et al. 2007; Lee et al. 2010). To date, however, it remains a challenging issue to measure the hyperelastic properties of soft materials in a local area or at small scales. Indentation proves to be a promising tool for such a purpose. Using the commercial indenter, indentation tests can be easily performed across different length scales. A key issue in indentation tests is to extract mechanical properties of materials from indentation responses, which represents an inverse problem and relies on the correlation between the material properties and indentation responses. During the past two decades, much effort has been directed toward developing robust methods to determine such properties as the elastic, elastoplastic, viscoelastic properties of materials using indentation tests (Oliver and Pharr 1992; Cheng and Cheng 2004; Fischer-Cripps 2011). This greatly facilitates the use of depth-sensing instrumented indentation for practical measurements.

In recent years, measuring the mechanical properties of hyperelastic materials using indentation tests has attracted considerable attention. For example, Lee et al. (2003) developed a spherical indentation approach to evaluate the material property of rubber materials described by the Yeoh model. Samani and Plewes (2004) proposed an inverse method to interpret the nonlinear indentation force–displacement response to measure the hyperelastic parameters of small

ex vivo tissue samples. Giannakopoulos and Triantafyllou (2007) addressed the spherical indentation of incompressible rubbery materials through theoretical and experimental efforts. Their theoretical analysis based on the Mooney–Rivlin model led to an analytical solution for the indentation load–depth curve with the ratio of the indentation depth to the indenter radius smaller than 10 %. Lin et al. (2009) proposed load–depth relations for a number of hyperelastic strain energy functions and validated the solutions for the ratio of the indentation depth to indenter radius smaller than 20 % via finite element simulations. Despite these advances, several fundamental issues as illustrated below regarding spherical indentation of hyperelastic solids remain, which deserve further effort.

First, indentation of hyperelastic solids usually involves coupled material, geometric, and boundary nonlinearity. Therefore, it is difficult to develop an analytical solution correlating the indentation responses and the material properties. Although several analytical solutions as aforementioned have been presented in the literature based on elastic contact theory for relatively small indentation depths (e.g., the ratio of indentation depth to indenter radius, $h/R < 0.2$), exploring the explicit expressions of the indentation load–depth curve valid up to large ratios of h/R is still an important issue and requires further investigation.

Second, extracting the hyperelastic properties of soft materials from indentation responses represents an inverse problem, which is usually ill-posed. According to Hadamard's definition (Hadamard 1923), an inverse problem is ill-posed if one of the following properties is not respected: (i) *there exists a solution to the problem* (**existence**), (ii) *no more than one solution exists* (**uniqueness**), and (iii) *the solution continuously depends on the data* (**stability**). To examine the extent to which the solution to an inverse problem can be reliably determined, one needs to explore its above properties. For spherical indentation of hyperelastic soft materials, however, there is no systematic investigation on the properties of the identified solution from the viewpoint of inverse problems.

Third, the nanoindentation technique based on Atomic Force Microscope (AFM) has been widely used to measure the mechanical properties of soft materials including soft tissues and cells (Cross et al. 2007; Crichton et al. 2011). Hertzian solution has been utilized by many authors to interpret the indentation data, which is based on the small deformation assumption and requires that the indentation depth should be much smaller than the tip radius. It has been shown that shallow depth indentation usually suffers from excessive noises which may preclude the accuracy of the measurement. Relatively larger indentation depth can help eliminate the data noise caused by surface effects. However, when the indented hyperelastic solid undergoes finite deformation, the initial elastic modulus identified using

Hertzian elastic contact theory may contain significant errors (Giannakopoulos and Triantafyllou 2007; Liu et al. 2010). Liu et al. (2010) argued that the hyperelastic solution reported by Giannakopoulos and Triantafyllou (2007) significantly overestimated the indentation load. But the big discrepancy between the Hertzian solution and the finite element results reported in their study (Liu et al. 2010) has not been well understood. In this sense, more systematic study is needed to identify the extent to which the Hertzian solution is applicable when the indented hyperelastic solid undergoes finite deformation.

Bearing the above issues in mind, in this paper, we explore the spherical indentation of hyperelastic solids through a combined effort of theoretical analysis, finite element simulations and experiments. The paper is organized as follows. In Sect. 2, four widely used hyperelastic models, including neo-Hookean, Mooney–Rivlin, Fung, and Arruda–Boyce model, are described, which will be used in our study. Section 3 carries out a dimensional analysis to characterize the relationship between the indentation responses and the hyperelastic properties of indented materials. Then, in Sect. 4, the closed-form expressions of the indentation load as a function of given indentation depths and the hyperelastic parameters are achieved based on large-scale finite element computations. In Sect. 5, the applicability of the Hertzian solution to the measurement of initial shear modulus of hyperelastic materials is examined. In Sect. 6, from the viewpoint of inverse problem, the possibility to measure some other properties (e.g., locking stretch) of a hyperelastic material is addressed by exploring the existence, uniqueness, and stability of the solution. Section 7 discusses the effects of friction and compressibility of the indented solid. Section 8 represents experiments conducted on polydimethylsiloxane (PDMS) to validate the results and conclusions given by theoretical analysis. Section 9 gives the concluding remarks.

2 Material models

In this study, we investigate four hyperelastic models, including neo-Hookean, Mooney–Rivlin, Fung, and Arruda–Boyce models, which have been widely applied to model the nonlinear deformation behavior of rubber-like materials and biological soft tissues. These models are briefly introduced as follows.

2.1 Mooney–Rivlin and neo-Hookean models

In the Mooney–Rivlin model, the strain energy function is written as (Mooney 1940; Rivlin 1948)

$$\Phi = C_{10} \left(\bar{I}_1 - 3 \right) + C_{01} \left(\bar{I}_2 - 3 \right) + \frac{1}{D} \left(J - 1 \right)^2, \qquad (1)$$

where Φ is the strain energy density per unit volume in the undeformed configuration, C_{10}, C_{01}, and D are material parameters and J the volume ratio. $\bar{I}_1$ and $\bar{I}_2$ are the first and second deviatoric strain invariants, with $\bar{I}_1 = \bar{\lambda}_1^2 + \bar{\lambda}_2^2 + \bar{\lambda}_3^2$ and $\bar{I}_2 = \bar{\lambda}_1^{-2} + \bar{\lambda}_2^{-2} + \bar{\lambda}_3^{-2}$, where $\bar{\lambda}_i$ is the deviatoric principal stretch which is related to the principal stretch λ_i by $\bar{\lambda}_i = J^{-\frac{1}{3}}\lambda_i$. The initial bulk modulus K_0 is related to D by $K_0 = \frac{2}{D}$, where $D = 0$ for incompressible materials. When $C_{01} \equiv 0$, Eq. (1) reduces to the strain energy density function of the neo-Hookean model

$$\Phi = C_{10}\left(\bar{I}_1 - 3\right) + \frac{1}{D}\left(J - 1\right)^2, \tag{2}$$

The initial shear modulus μ_0 is given by $\mu_0 = 2(C_{10} + C_{01})$ for Mooney–Rivlin model and $\mu_0 = 2C_{10}$ for neo-Hookean model. Poisson's ratio is related to the bulk modulus and the initial shear modulus by $\nu = \frac{3K_0 - 2\mu_0}{6K_0 + 2\mu_0}$.

2.2 Arruda–Boyce model

Arruda–Boyce model (Arruda and Boyce 1993), also known as the eight-chain model, is developed based on an eight-chain representation of the underlying macromolecular network structure of rubber and the non-Gaussian behavior of the chains in the network. The strain energy density function in this model is given by

$$\begin{aligned}\Phi = \mu &\left\{\frac{1}{2}\left(\bar{I}_1 - 3\right) + \frac{1}{20\lambda_m^2}\left(\bar{I}_1^2 - 9\right)\right.\\&+ \frac{11}{1050\lambda_m^4}\left(\bar{I}_1^3 - 27\right) + \frac{19}{7000\lambda_m^6}\left(\bar{I}_1^4 - 81\right)\\&+ \left.\frac{519}{673750\lambda_m^8}\left(\bar{I}_1^5 - 243\right)\right\} + \frac{1}{D}\left(\frac{J^2 - 1}{2} - \ln J\right),\end{aligned}\tag{3}$$

This model captures the cooperative nature of network deformation with only two material parameters, i.e., the shear modulus μ and locking stretch λ_m. The two parameters are linked to the physics of molecular chain orientations involved in the deformation of rubbery materials and elastomers. In this model, the initial shear modulus μ_0 is related to the shear modulus μ via the expression

$$\mu_0 = \mu\left(1 + \frac{3}{5\lambda_m^2} + \frac{99}{175\lambda_m^4} + \frac{513}{875\lambda_m^6} + \frac{42039}{67375\lambda_m^8}\right), \tag{4}$$

where λ_m can be obtained by

$$\lambda_m = \sqrt{\frac{1}{3}\left(\lambda_{\text{lim}}^2 + \frac{2}{\lambda_{\text{lim}}}\right)}. \tag{5}$$

λ_{lim} is the limit chain representing the stretch at which the stress starts to increase without limit.

2.3 Fung model

Fung et al. (1979) proposed a hyperelastic model to describe the nonlinear deformation behavior of biological soft tissues, in which the strain energy function reads

$$\Phi = \frac{C}{2b}\left(e^{b(\bar{I}_1 - 3)} - 1\right) + \frac{1}{D}\left(\frac{(J)^2 - 1}{2} - \ln J\right), \tag{6}$$

where C and b are material parameters. In this model, the initial shear modulus is given by $\mu_0 = C$.

3 Dimensional analysis

Dimensional analysis is a useful tool to analyze the indentation tests (Cheng and Cheng 1998, 2004; Dao et al. 2001). It states that a physical law does not depend on the arbitrariness in the choice of units of physical quantities. Consequently, the functions expressing the physical law must process certain mathematical property, called generalized homogeneity, i.e., each of the additive terms in the functions will have the same dimensions or units. This concept often allows the number of arguments in the mathematical expressions describing physical phenomena to be reduced. This basic idea leads to the central theorem in dimensional analysis, i.e., the so-called PI-theorem (or Π theorem) (Barenblatt 1996). This theorem describes how a physically meaningful equation involving k variables can be equivalently rewritten as an equation of k-m dimensionless parameters, where m is the number of variables with independent dimensions. Most importantly, it provides a method for computing these dimensionless parameters from the given variables, even if the form of the equation is still unknown.

Scaling relations given by dimensional analysis not only provide insight into the shape of indentation load–depth curves, but also provide guidelines for finite element modeling of indentation tests. Particularly, when only a few geometric and physical parameters are involved (e.g., for the constitutive models under study), the combination of dimensional analysis with finite element simulations permits to develop explicit expressions for the relationship between the indentation responses and material properties (Cheng and Cheng 2004).

In the present paper, the dimensional analysis method is used to study the spherical indentation of incompressible or weakly compressible hyperelastic materials with constitutive relations described in Sect. 2. For the spherical indentation of an incompressible neo-Hookean solid, the indentation load P must be a function of the following independent parameters:

$$P_{\text{nH}} = f\left(\mu_0, h, R\right), \tag{7}$$

where μ_0 is the shear modulus at ground state, h the indentation depth, and R the indenter radius. Applying Π theorem to Eq. (7) gives

$$P_{\mathrm{nH}} = \mu_0 \sqrt{Rh} h \Pi_{\mathrm{nH}} \left(\frac{h}{R} \right), \tag{8}$$

where Π_{nH} is a dimensionless function, which can be determined by finite element simulations, as shown in the sequel.

Adopting dimensional analysis to the spherical indentation of a Mooney–Rivlin solid, the indentation load P_{MR} may be expressed as

$$P_{\mathrm{MR}} = \mu_0 \sqrt{Rh} h \Pi_{\mathrm{MR}} \left(\Theta, \frac{h}{R} \right), \tag{9}$$

where Π_{MR} is a dimensionless function and $\Theta = C_{01}/(C_{01} + C_{10})$.

Similarly, the indentation load–depth relations for the Arruda–Boyce and Fung models are, respectively, given by

$$P_{\mathrm{AB}} = \mu_0 \sqrt{Rh} h \Pi_{\mathrm{AB}} \left(\lambda_m, \frac{h}{R} \right), \tag{10}$$

$$P_{\mathrm{F}} = \mu_0 \sqrt{Rh} h \Pi_{\mathrm{F}} \left(b, \frac{h}{R} \right), \tag{11}$$

where Π_{AB} and Π_{F} are dimensionless functions. At a given ratio of indentation depth to indenter radius h_g/R, Eqs. (9)–(11) reduce to

$$P_{\mathrm{MR},g} = \mu_0 \sqrt{Rh_g} h_g \Pi_{\mathrm{MR}} (\Theta), \tag{12a}$$

$$P_{\mathrm{AB},g} = \mu_0 \sqrt{Rh_g} h_g \Pi_{\mathrm{AB}} (\lambda_m), \tag{12b}$$

$$P_{\mathrm{F},g} = \mu_0 \sqrt{Rh_g} h_g \Pi_{\mathrm{F}} (b). \tag{12c}$$

Clearly, once the dimensionless functions are known, the correlations between the indentation loads at the given indentation depths and material properties are determined. In next section, we will identify the closed-form expressions of the dimensionless functions in Eqs. (8) and (12) for the ratio of h_g/R varying in a wide range.

4 Closed-form relations between indentation responses and material properties

To identify the closed-form expressions of the dimensionless functions in Eqs. (8) and (12), nonlinear finite element computations are carried out in this section using ABAQUS (2009). We consider the material, geometric, and boundary nonlinearity involved in the problem simultaneously. The nonlinear finite element simulations also allow us to determine the dimensionless functions in Sect. 3 at large ratios of h/R, (e.g., $h/R = 1$), which is difficult to derive by analytical methods. We implanted the Fung model into ABAQUS via the user subroutine **UHYPER**. The other three hyperelastic models introduced in Sect. 2 have already been included

Table 1 Material parameters used in the simulations

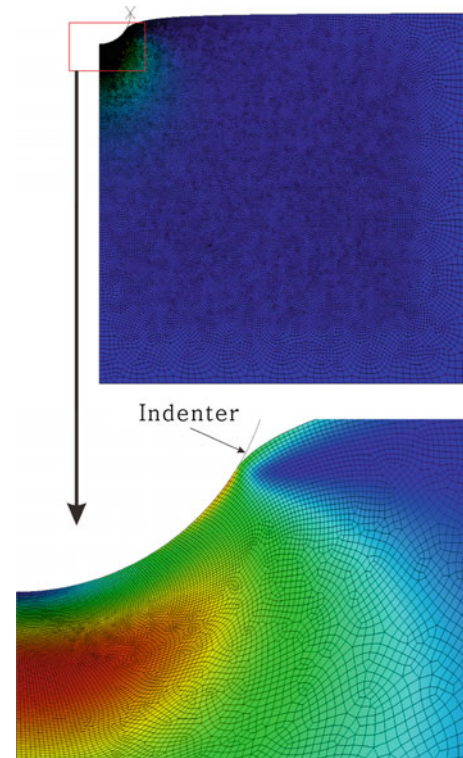| Model	Parameters	Range of parameters
Mooney–Rivlin	$\Theta = \frac{C_{01}}{C_{10} + C_{01}}$	[0, 1]
Fung	b	[0.04, 1.00]
Arruda–Boyce	λ_m	[1, 10]

Fig. 1 Finite element mesh used in computational studies

in ABAQUS and can be used directly. The parameters used in this study are taken according to the literature and vary in wide ranges of practical interest, as listed in Table 1. The value of the initial modulus μ_0 can be taken arbitrarily in the determination of the dimensionless functions in Sect. 3 and is taken as 1 MPa in our simulations.

An axisymmetric model is adopted here and a total of 41121 four-node bilinear axisymmetric reduced integration elements are used to discretize the semi-infinite substrate of the indented solid. The boundary conditions are that the outer surface nodes are traction-free and the lower surface nodes are fixed. The indenter is assumed to be rigid, with the radius $R = 2.5$ mm. The maximum ratio of the indentation depth to indenter radius is taken as $h/R = 1$. The spherical indenter and the finite element model used in the present analysis are schematically showed by Fig. 1. Friction is omitted here but its effects will be examined in the sequel. Convergence of the computation was guaranteed by comparing the present

Table 2 The coefficients corresponding to various h_g/R for Mooney–Rivlin

h_g/R	0.01	0.03	0.05	0.07	0.1	0.3	0.5	0.7	1
C_1	5.317013	5.293920	5.276747	5.260480	5.236587	5.087467	4.936427	4.780693	4.534187
C_2	0.072213	0.128747	0.164533	0.196693	0.240640	0.448587	0.625973	0.796747	1.068427
C_3	−0.001238	−0.003277	−0.002632	−0.004346	−0.008800	−0.028320	−0.055893	−0.089173	−0.158827

Table 3 The coefficients corresponding to various h_g/R for Fung

h_g/R	0.01	0.03	0.05	0.07	0.1	0.3	0.5	0.7	1
D_1	5.316960	5.293867	5.277067	5.260747	5.236640	5.086933	4.935733	4.779840	4.534187
D_2	0.006720	0.018080	0.025707	0.036693	0.055360	0.183200	0.335893	0.519840	0.871360
D_3	−0.000108	−0.000321	0.001763	0.001709	0.000721	−0.006400	−0.018827	−0.044373	−0.121920

Table 4 The coefficients corresponding to various h_g/R for Arruda–Boyce

h_g/R	0.01	0.03	0.05	0.07	0.1	0.3	0.5	0.7	1
A_0	5.317013	5.293920	5.277067	5.260800	5.236960	5.087413	4.936640	4.784427	4.538613
A_1	0.041120	0.039307	0.176960	0.112853	0.384107	0.866720	0.044907	1.097867	1.577920
B_1	0.320670	0.321500	0.318160	0.319080	0.306880	0.328940	1.701070	0.410720	0.433900
A_2	0.001092	0.164107	0.134240	0.322720	0.010827	0.028267	1.633973	1.097867	1.577920
B_2	1.529220	0.321490	0.318170	0.319080	1.405770	1.587670	0.338240	0.410720	0.433900
A_3	0.034347	0.002908	0.004629	0.006560	0.335733	1.051893	1.617120	1.097867	1.577920
B_3	0.320670	1.566670	1.500330	1.502030	0.306890	0.328930	0.338230	0.410720	0.433900

results with those calculated using a refined mesh (71319 four-node bilinear axisymmetric elements).

Based on the computational results, the dimensionless function $\Pi_{nH}\left(\frac{h}{R}\right)$ in Eq. (8) is determined as

$$\Pi_{nH}\left(\frac{h}{R}\right) = \frac{16}{3}\left(1 - 0.15\frac{h}{R}\right), \qquad (13)$$

Equations (8) and (13) give an explicit expression of the indentation load–depth curve for the spherical indentation of neo-Hookean solid

$$P_{nH} = \frac{16}{3}\mu_0\sqrt{Rh}h\left(1 - 0.15\frac{h}{R}\right), \qquad (14)$$

which is valid up to $h/R = 1$.

At a number of different ratios of indentation depth to indenter radius (i.e., h_g/R varies from 0.01 to 1), the closed-form expressions of the dimensionless functions Π_{MR}, Π_F, and Π_{AB} are obtained as

$$\Pi_{MR}(\Theta) = C_1 + C_2\Theta + C_3\Theta^2, \qquad (15a)$$

$$\Pi_F(b) = D_1 + D_2 b + D_3 b^2, \qquad (15b)$$

$$\Pi_{AB}(\lambda_m) = A_0 + \sum_{i=1}^{3} A_i e^{-\lambda_m/B_i}, \qquad (15c)$$

respectively, where C_i and D_i $(i = 1, 2, 3)$ are constants and given in Tables 2 and 3 for different ratios of h_g/R.

A_0, A_i, and B_i, $(i = 1, 2, 3)$, are constants and given in Table 4.

5 Applicability of Hertzian solution to determining the initial shear modulus of hyperelastic solids

The closed-form solutions developed in Sect. 4 enable us to examine the applicability of Hertzian solution to the determination of the initial shear modulus of hyperelastic solids. When the indented solid is incompressible, Hertzian solution gives the indentation load–depth relation as

$$P_H = \frac{16}{3}\mu_0\sqrt{Rh}h, \qquad (16)$$

For a neo-Hookean solid, normalizing the indentation load (Eq. 8) by Hertzian solution (Eq. 16) gives

$$\frac{P_{nH}}{P_H} = \frac{3\Pi_{nH}(h/R)}{16} = 1 - 0.15\frac{h}{R}, \qquad (17)$$

Equation (17) shows that when $h/R = 1$, the difference between P_H and P_{nH} is up to 15 %; when $h/R \leq 0.3$, the difference between P_H and P_{nH} is smaller than 5 %. At a given indentation depth, it is known from Eqs. (12)–(16) that
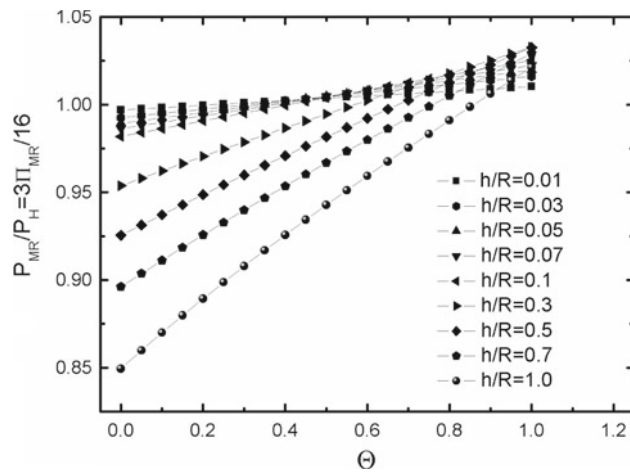
Fig. 2 Dependence of the dimensionless function Π_{MR} on the parameter Θ and ratios of h/R

Fig. 3 Dependence of the dimensionless function Π_F on the parameter b and ratios of h/R

$$\frac{P_{MR,g}}{P_H} = \frac{3}{16}\Pi_{MR}(\Theta) \text{ (Mooney−Rivlin model)}, \quad (18a)$$

$$\frac{P_{AB,g}}{P_H} = \frac{3}{16}\Pi_{AB}(\lambda_m) \text{ (Arruda−Boyce model)}, \quad (18b)$$

$$\frac{P_{F,g}}{P_H} = \frac{3}{16}\Pi_F(b) \quad \text{(Fung model)}, \quad (18c)$$

Based on Eqs. (15), (17), and (18), the normalized indentation loads at different ratios of h_g/R for the three hyperelastic models are plotted in Figs. 2, 3 and 4. From the results for Mooney–Rivlin, Fung, and Arruda–Boyce models, it can be found that for a hyperelastic material with a small locking stretch (i.e., when λ_m in Arruda–Boyce model is small or b in Fung model is large), the difference between the Hertzian solution and the solutions developed based on nonlinear analysis is relatively small. When the locking stretch of the material is large, the results based on Mooney–Rivlin, Fung, and Arruda–Boyce models are quite similar to that for the neo-Hookean model. In this case, our computational results show that the difference between the Herzian solution and the hyperelastic indentation solutions is around 15 % when $h/R = 1$.

It can be concluded from the above results that when the ratio of the indentation depth to the indenter radius is smaller than 0.2, Hertzian solution can be reliably adopted to determine the initial shear modulus of incompressible hyperelastic solids. When indentation depth is large, e.g., $h/R > 0.5$, Hertzian solution underestimates the initial shear modulus of a hyperelastic solid, which can be modeled using neo-Hookean, Mooney–Rivlin, Fung or Arruda–Boyce model. The larger the locking stretch of an indented solid, the greater the error in the initial shear modulus given by Hertzian solution. When the locking stretch is large, the hyperelastic solution developed in this study (e.g., Eq. 14) provides a more accurate solution for evaluating the initial shear modulus.
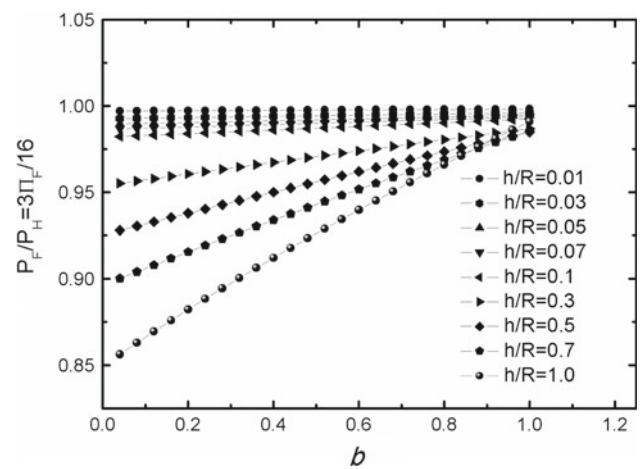

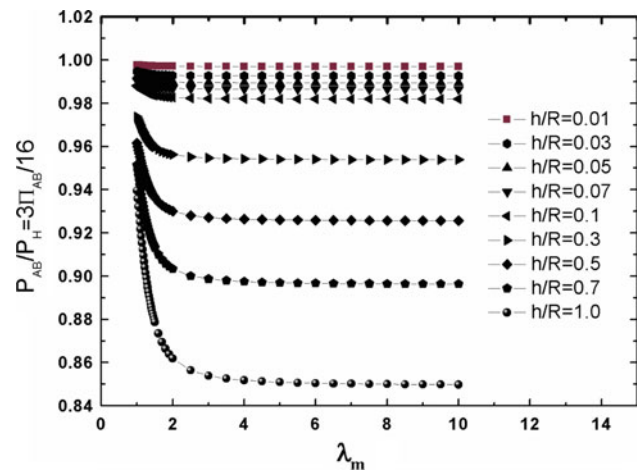**Fig. 4** Dependence of the dimensionless function Π_{AB} on the parameter λ_m and ratios of h/R

6 Determination of other hyperelastic parameters of soft materials

The results in Sect. 5 show that the initial shear modulus can be determined using spherical indentation tests with a good accuracy. In this section, we explore whether the spherical indentation method permits to determine other hyperelastic properties of hyperelastic solids reliably, e.g., parameter Θ in Mooney–Rivlin model, λ_m in Arruda–Boyce model, and b in Fung model. Determining the properties of hyperelastic solids represents an inverse problem. As aforementioned, an inverse problem may be ill-posed. Therefore, we need to explore the properties of the inverse problem under study, i.e., the existence, uniqueness, and stability of the solution. Since the initial shear modulus μ_0 can be determined with a good accuracy using data corresponding to a relatively small h/R, we explore here whether other hyperelastic properties can be determined from the indentation load–depth relations

given by Eq. (12). *Existence* and *uniqueness* of the solution to an inverse problem are mainly determined by the properties of the operators. A careful examination on the properties of the operators given by Eqs. (12) and (15) shows that the *existence* and *uniqueness* of the solution can be guaranteed in theory. However, it should be noted that the solution may not exist provided that the input data are polluted by significant errors. In practice, the condition of *stability* is most often violated and deserves more attention. The lack of *stability* can cause the computed solution to an inverse problem to have nothing to do with the true solution. Careful attention must therefore be paid to this aspect. It should be pointed out that *uniqueness* and *stability* are two fundamentally different concepts in the mathematic theory of inverse problems. The former is determined by the property of the operator, i.e., the form of the dimensionless function in the present study, whereas the latter relies on how the solution depends on the input data. In this section, we focus on the stability of the solution of the present problem by exploring its condition number, which quantitatively measures the sensitivity of the identified solution to data errors. For example, when the condition number is 5, an error of 3 % in the input data will lead to an error of 15 % in the identified solution. A problem is ill-conditioned if the condition number is large and it is ill-posed if the condition number is infinity (Hadamard 1923).

Based on Eq. (12), the condition numbers for the determination of the parameters Θ, λ_m, and b can be defined as (Cao and Lu 2004a,b)

$$\Psi_{MR} = \frac{\Delta\Theta}{\Theta} \bigg/ \frac{\Delta\Pi_{MR}}{\Pi_{MR}} = \frac{\Pi_{MR}}{\Theta\Pi'_{MR}(\Theta)}, \qquad (19a)$$

$$\Psi_{AB} = \frac{\Delta\lambda_m}{\lambda_m} \bigg/ \frac{\Delta\Pi_{AB}}{\Pi_{AB}} = \frac{\Pi_{AB}}{\lambda_m\Pi'_{AB}(\lambda_m)}, \qquad (19b)$$

$$\Psi_{F} = \frac{\Delta b}{b} \bigg/ \frac{\Delta\Pi_{F}}{\Pi_{F}} = \frac{\Pi_{F}}{b\Pi'_{F}(b)}, \qquad (19c)$$

where $\Pi'_{MR}(\Theta) = d\Pi_{MR}/d\Theta$, $\Pi'_{AB}(\lambda_m) = d\Pi_{AB}/d\lambda_m$, $\Pi'_{F}(b) = d\Pi_{F}/db$. From Eqs. (12), (15) and (19), the closed-form expressions of the condition numbers defined above can be obtained. For the Mooney–Rivlin model, the condition number is

$$\Psi_{MR} = \frac{\Pi_{MR}}{\Theta\Pi'_{MR}(\Theta)} = \frac{C_1 + C_2\Theta + C_3\Theta^2}{C_2\Theta + 2C_3\Theta^2}, \qquad (20)$$

The closed-form expression of the condition number for Fung model is the same as Eq. (20), with the constants C_i ($i = 1, 2, 3$) replaced by D_i, and the variable Θ replaced by b, respectively. According to Eqs. (12), (15), and (19c), the condition number for the Arruda–Boyce model can be expressed in the following closed-form:

$$\Psi_{AB} = \frac{\Pi_{AB}}{\lambda_m\Pi'_{AB}(\lambda_m)} = \frac{A_0 + \sum_{i=1}^{3} A_i e^{-\lambda_m/B_i}}{\lambda_m \sum_{i=1}^{3} \left(\frac{-A_i}{B_i} e^{-\lambda_m/B_i}\right)}. \qquad (21)$$
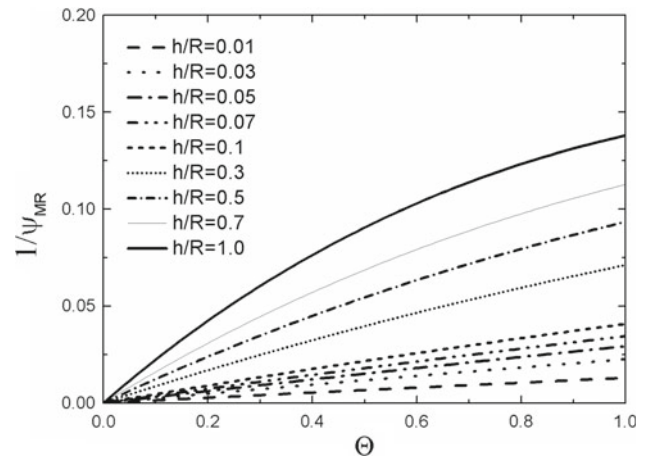

Fig. 5 Condition numbers for the determination of Θ corresponding to different ratios of h/R
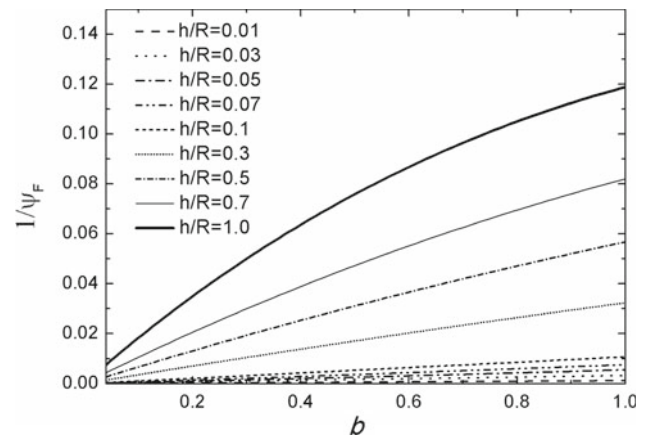

Fig. 6 Condition numbers for the determination of the parameter b using the data corresponding to different ratios of h/R

The explicit results derived here permit to quantitatively examine the extent to which the parameters Θ, b, and λ_m can be determined using spherical indentation tests. Figures 5, 6, and 7 illustrate the variation in the condition numbers for the three hyperelastic models for various values of h/R. We can obtain the following insightful information.

(i) At a given indentation depth, the condition numbers decrease with the parameters Θ, b and increase with λ_m. This indicates that for a hyperelastic material with a small locking stretch, e.g., many biological soft tissues (Fung 1993), the aforementioned hyperelastic parameters may be determined using spherical indentation.

(ii) For the determination of the parameters Θ, b and λ_m, the condition numbers decrease with the indentation depth. Therefore, application of the data corresponding to a large ratio of h/R may provide more reliable evaluation on these parameters. But it is pointed out that a large ratio of h/R corresponds to a high strain level, and in this case,
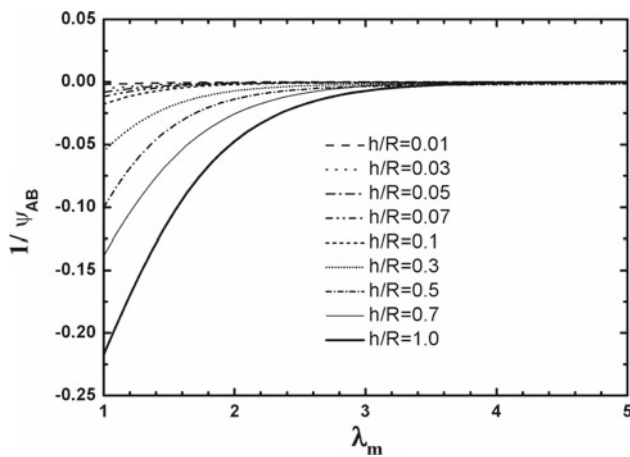
Fig. 7 Condition numbers for the determination of the parameter λ_m using the data corresponding to different ratios of h/R

Fig. 8 Effects of friction on the indentation responses

Fig. 9 Effects of compressibility of the indented material on the computational results, Poisson's ratio is taken as 0.48

indentation may cause the damage of the indented solid in the measurements of some fragile materials. Caution should be paid to this aspect in the practical use of the method proposed here.

7 Effects of friction and compressibility of the indented substrate

The above analysis assumes that the indenter/substrate interface is frictionless and the indented hyperelastic solid is incompressible. In this section, we explore the effects of friction and compressibility of the indented solid on the conclusions drawn in Sects. 5 and 6. Arruda–Boyce model is taken as an example.

The computational model is the same as that described in Sect. 4. We simulate the frictional contact of the indenter with the indented solid by taking the friction coefficient as 0.1. Figure 8 shows the comparison of the indentation load–depth curve with that in the frictionless contact case for several representative locking stretches λ_m. Hertzian solution is also included in the figure for comparison. It can be seen from the results that friction does not have significant influence on the indentation load–depth curve of a hyperelastic material, and the difference between the results of the frictional and frictionless contact is smaller than 2 %.

We further explore the case in which the indented solid is weakly compressible. The Poisson's ratio ν is taken as 0.48, and the parameter D in the hyperelastic models is related to the Poisson's ratio by $D = \frac{3(1-2\nu)}{\mu_0(1+\nu)}$. Since ν is taken as constant, the results given by dimensional analysis, i.e., Eqs. (9) and (12), remain valid. The dimensionless functions are determined from the computational results. The indentation loads at a number of given indentation depths are compared with the Hertzian solution in Fig. 9. The results are quite sim-
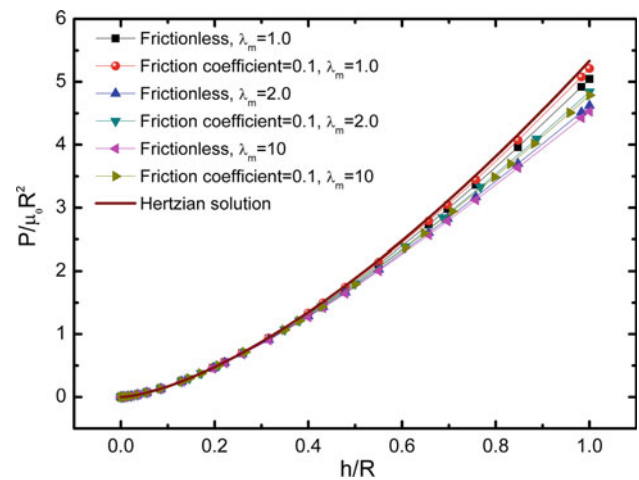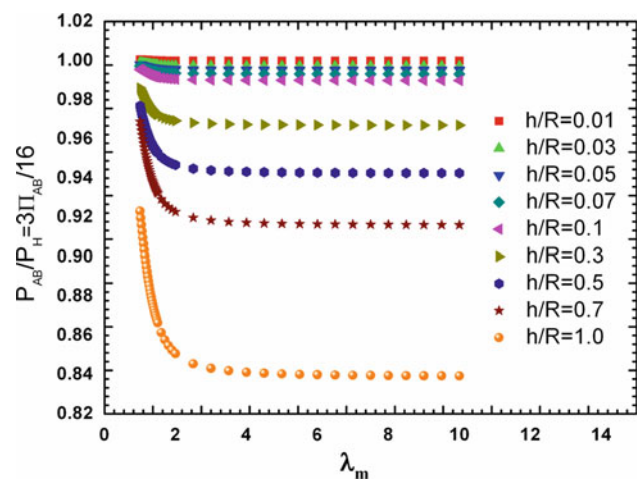
ilar to those for the incompressible substrate, and therefore the conclusions drawn in Sects. 5 and 6 for incompressible indented solid are still valid for weakly compressible substrates.

8 Experiments

In this section, experiments are carried out to validate the conclusions given by theoretical analysis and the computational studies. Polydimethylsiloxane (PDMS) is prepared by mixing a degassed elastomer base and a crosslinker at a ratio of 20:1 w/w. The pre-polymerized mixture is filled in a cylindrical mold and cured at 60 °C for 8 h. When the PDMS becomes a solid, it is taken out to prepare experimental specimens for both tension and indentation tests. The ElectroForce® 3100 test instrument (Bose, Fig. 10) is used for the measurements. The machine can reach a maximum load of 22 N. The
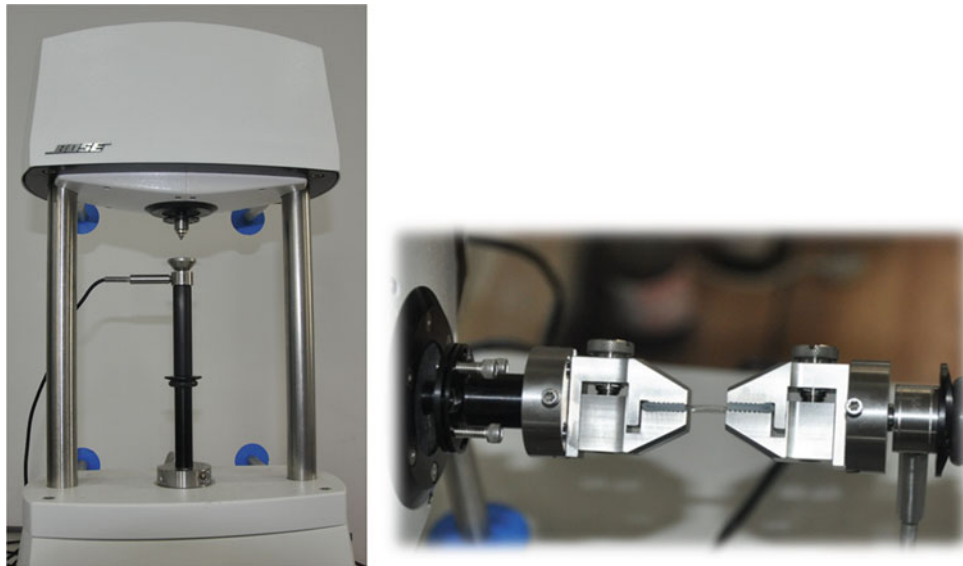
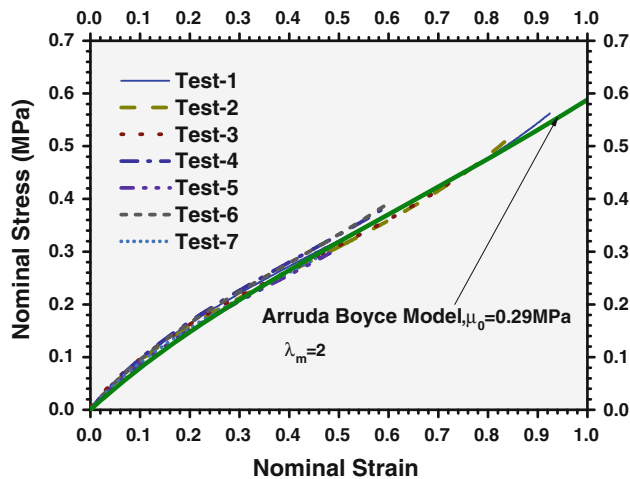**Fig. 10** The ElectroForce® 3100 test instrument used in our experiments

Fig. 11 Stress–strain curves given by tensile tests

Fig. 12 Indentation loading curves measured at six different positions of the sample

displacement resolution is 1 μm and the load resolution is 0.5 mN.

Tensile tests are first performed. The specimen has a width of 2.48 mm and a thickness of 2.46 mm. The gauge lengths of the specimens vary from 4.76 to 9.62 mm. Displacement controlled loading procedure is applied and the measurements conducted at ambient temperature (23 °C) with the humidity of around 50 %. The loading rate is taken as 2 mm/s, which is sufficiently large to ensure that the effect of viscosity of the material was negligible. The nominal stress–strain curves are given in Fig. 11. The initial shear modulus directly given by the nominal stress–strain curves is 0.31 ± 0.02 MPa. Fitting the nominal stress–strain curve with Arruda–Boyce model gives the initial shear modulus $\mu_0 = 0.29$ MPa and the locking stretch $\lambda_m = 2.1$.
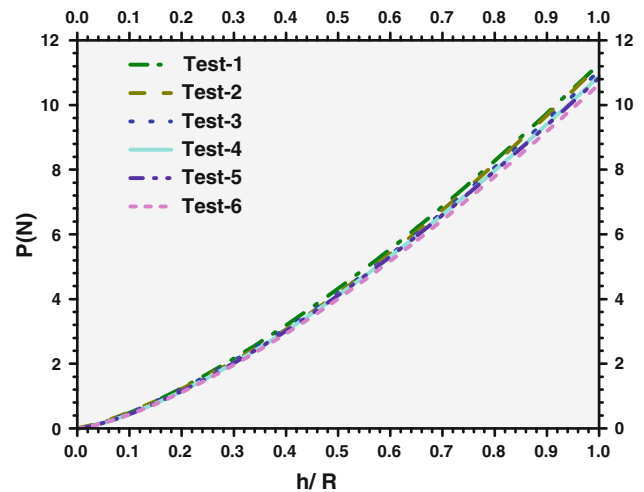
The ElectroForce® 3100 test instrument is also used for the indentation tests. A spherical indenter with a radius of 3 mm was adopted. The measurements are also performed at room temperature (23 °C) and a humidity of about 50 %. Displacement controlled loading procedure is applied. The loading rate is set as 2 mm/s and the maximum indentation depth is 3 mm. The sample has a diameter of 55 mm and a height of 31 mm. Six measurements at different positions of the sample are conducted, and the indentation load–depth curves are given in Fig. 12. The initial shear modulus is determined by fitting the load curves up to different ratios of h/R using Hertzian solution and the hyperelastic solution (Eq. 14), respectively, the values are given in Table 5.

Table 5 The initial shear modulus obtained by fitting the indentation loading curve up to different ratios of h_m/R using Hertzian solution and the hyperelastic solution (Eq. 14), where h_m is the maximum indentation depth taken in data analysis

h_m/R	μ_0(MPa) given by Hertzian solution	μ_0(MPa) given by Eq. (14)
0.2	0.303	0.311
0.4	0.273	0.288
0.6	0.255	0.276
0.8	0.249	0.273
1.0	0.246	0.271

Comparing the initial shear moduli determined from tension and indentation tests, we find that when the indentation depth is large, the Hertzian solution underestimates the initial shear modulus of a hyperelastic solid, as predicted by our theoretical analysis. The initial shear moduli inversely determined by using the hyperelastic solution are slightly depth-dependent, but clearly they are closer to those given by tensile tests. Using the experimental data and Eqs. (12b) and (15c), we do not successfully identify a reasonable locking stretch of the indented material, which is around 2 according to the tensile tests. This is mainly due to that the experimental errors cannot be avoided, and the identified locking stretch is very sensitive to data noise when it is not close to 1 as revealed by our theoretical result shown in Fig. 7.

9 Concluding remarks

In this paper, we have explored the spherical indentation of hyperelastic soft materials via dimensional analysis method, finite element simulations and experiments. The key results of this study are summarized as follows.

First, for four widely used hyperelastic models, i.e., neo-Hookean, Mooney–Rivlin, Fung, and Arruda–Boyce model, we have proposed a general method based on dimensional analysis method and finite element simulations to establish explicit expressions of the relationship between material properties and indentation responses. Such a method is applicable when the indentation depth is comparable to or even greater than the indenter radius.

Second, based on the obtained explicit results, we have addressed the applicability of Hertzian solution to determine the initial shear modulus of a hyperelastic solid. Our results show that the initial shear modulus could be reliably determined using Hertzian solution provided that the ratio of the indentation depth to indenter radius is smaller than 0.2. The larger the locking stretch, the greater the error in the identified results using Hertzian solution. When the locking stretch of the indented material is large, the error in the identified results based on Hertzian solution can be up to 15 % for $h/R = 1$; in this case, the solution developed in this study (Eq. 14) could give more accurate results.

Third, the possibility to determine other hyperelastic properties besides the initial shear modulus has been studied by exploring the properties of the inverse problems, i.e., the existence, uniqueness, and stability of the solution. To this end, the condition numbers for the determination of such parameters as Θ, b, and λ_m in Mooney–Rivlin, Fung, and Arruda–Boyce models, respectively, have been defined and their explicit forms have been derived. It can be drawn from our theoretical analysis that only when the parameters Θ and b are large or λ_m is small (e.g., most biological soft tissues), they may be determined using spherical indentation responses at large ratios of h/R. Otherwise, these hyperelastic parameters given by spherical indentation tests are very sensitive to data errors. A reliable determination of these parameters usually requires that the indented solid undergoes sufficiently large deformation in indentation tests. Toward this end, profiting the effects of a rigid substrate to induce large deformation in the indented sample appears to be a promising route, which has received attention recently (Chen and Diebels 2012). But in this case, correlations between the indentation responses and material properties in explicit form have not been established and require more effort. Besides, only one or two material parameters are involved in the present inverse problems, when more mechanical parameters are involved, the problem will be more complicated and the inverse procedure may not only suffer from the *stability* issue but also the *existence* and *uniqueness* issues. Effects of friction and compressibility of the indented substrate are also discussed. It is found that the above conclusions apply to the case where the friction is in presence and the indented solid is weakly compressible.

Finally, experiments have been conducted on PDMS (1:20). The results reveal an underestimation of the initial shear modulus when Hertzian solution is used to fit the indentation loading curve up to a large ratio of indentation depth to indenter radius. Instead, the initial shear modulus evaluated by fitting the load–depth curve using the hyperelastic solution is more accurate. This is basically consistent with our theoretical analysis. It is emphasized here that we proposed the results for four commonly used hyperelastic models. When using the methods developed here to analyze the indentation response of a hyperelastic solid, one needs first to choose a suitable constitutive model.

References

ABAQUS (2009) ABAQUS user's manual, version 6.9

Arruda EM, Boyce MC (1993) A three-dimensional constitutive model for the large stretch behavior of rubber elastic materials. J Mech Phys Solids 41:389–412

Barenblatt GI (1996) Scaling, self-similarity, and intermediate asymptotics. Cambridge University Press, Cambridge, MA

Ben Amar M, Goriely A (2005) Growth and instability in elastic tissues. J Mech Phys Solids 53:2284–2319

Cao YP, Lu J (2004a) Depth-sensing instrumented indentation with dual sharp indenters: stability analysis and corresponding regularization schemes. Acta Mater 52:1143–1153

Cao YP, Lu J (2004b) A new method to extract the plastic properties of metal materials from an instrumented spherical indentation loading curve. Acta Mater 52:4023–4032

Cheng YT, Cheng CM (1998) Relationships between hardness, elastic modulus, and the work of indentation. Appl Phys Lett 73:614–616

Cheng YT, Cheng CM (2004) Scaling, dimensional analysis, and indentation measurements. Mater Sci Eng R-Rep 44:91–149

Chen ZY, Diebels S (2012) Nanoindentation of hyperelastic polymer layers at finite deformation and parameter re-identification. Arch Appl Mech 82:1041–1056

Crichton ML, Donose BC, Chen X, Raphael AP, Huang H, Kendall MAF (2011) The viscoelastic, hyperelastic and scale dependent behaviour of freshly excised individual skin layers. Biomaterials 32:4670–4681

Cross SE, Jin YS, Rao JY, Gimzewski JK (2007) Nanomechanical analysis of cells from cancer patients. Nat Nanotech 2:780–783

Dao M, Chollacoop N, Van Vliet KJ, Venkatesh TA, Suresh S (2001) Computational modeling of the forward and reverse problems in instrumented sharp indentation. Acta Mater 49:3899–3918

Fischer-Cripps AC (2011) Nanoindentation. Springer, New York

Fung YC (1993) Biomechanics: mechanical properties of living tissues. Springer, New York

Fung YC, Fronek K, Patitucci P (1979) Pseudoelasticity of arteries and the choice of its mathematical expression. Am J Physiol-Heart C 237:H620–H631

Giannakopoulos AE, Triantafyllou A (2007) Spherical indentation of incompressible rubber-like materials. J Mech Phys Solids 55:1196–1211

Hadamard J (1923) Lectures on Cauchy's problems in linear partial differential equations. Yale University Press, New Haven, CT

Holzapfel GA, Ogden RW (2006) Mechanics of biological tissue. Springer, Berlin

Humphrey JD (2003) Continuum biomechanics of soft biological tissues. Proc R Soc A 459:3–46

Lee B, Han L, Frank EH, Chubinskaya S, Ortiz C, Grodzinsky AJ (2010) Dynamic mechanical properties of the tissue-engineered matrix associated with individual chondrocytes. J Biomech 43:469–476

Lee H, Pharr GM, Nahm SH (2003) Material property evaluation of hyper-elastic rubber by micro-indentation. In: Proceedings of the SEM annual conference and exposition on experimental and applied mechanics

Levental I, Georges PC, Janmey PA (2007) Soft biological materials and their impact on cell function. Soft Matter 3:299–306

Li B, Cao YP, Feng XQ, Gao H (2012) Mechanics of morphological instabilities and surface wrinkling in soft materials: a review. Soft Matter 8:5728–5745

Lin D, Shreiber D, Dimitriadis E, Horkay F (2009) Spherical indentation of soft matter beyond the Hertzian regime: numerical and experimental validation of hyperelastic models. Biomech Model Mech 8:345–358

Liu D, Zhang Z, Sun L (2010) Nonlinear elastic load-displacement relation for spherical indentation on rubberlike materials. J Mater Res 25:2197–2202

Mooney M (1940) A theory of large elastic deformation. J Appl Phys 11:582–592

Oliver WC, Pharr GM (1992) Improved technique for determining hardness and elastic modulus using load and displacement sensing indentation experiments. J Mater Res 7:1564–1583

Rivlin RS (1948) Large elastic deformations of isotropic materials. IV. Further developments of the general theory. Philos Trans R Soc Lond Ser A Math Phys Sci 241:379–397

Rodriguez EK, Hoger A, McCulloch A (1994) Stress-dependent finite growth in soft elastic tissue. J Biomech 27:455–467

Samani A, Plewes D (2004) A method to measure the hyperelastic parameters of *ex vivo* breast tissue samples. Phys Med Biol 49:4395–4405

Taber LA (1995) Biomechanics of growth, remodeling, and morphogenesis. Appl Mech Rev 48:487–545